

Study of Multiple Plasmon Resonance based Broadband Cross-Polarization Conversion on an Anisotropic Metasurface

Tanu Singh Sisodia*, B. P. Singh,

Department of Physics, Dr. Bhimrao Ambedkar University, Agra (U.P.), India

Abstract - This paper presents the design and simulation of a broadband microwave Cross-Polarization-Conversion (CPC) metasurface. The metasurface is composed of a Split Ring Resonator (SRR) with two splits placed on perpendicular sides, and a Circular Splitted Ring Resonator (C-SRR) printed over a copper-backed FR4 dielectric substrate within these splits. The simulation results demonstrate that the metasurface exhibits excellent CPC performance, achieving a 3 dB fractional bandwidth of up to 73% over the frequency range of 5 to 15 GHz, for both normal and oblique incidences. The metasurface's response is unaffected by the incidence angle and polarization of the incoming wave due to its symmetric structure and sub-wavelength unit cell size. This makes it a promising candidate for practical applications. Multiple plasmonic resonances at three distinct frequencies (5.5 GHz, 8.2 GHz, and 14.1 GHz) contribute to the broadband polarization conversion exhibited in this study. The numerical and simulation results of the proposed design have been validated.

Key Words: Metasurface, Plasmon resonances, Anisotropy, Cross-Polarization Conversion (CPC).

1. INTRODUCTION

Recent research has reported successful polarization conversion across different frequency ranges of the electromagnetic spectrum, employing various geometric elements. For instance, plasmonic nano-rods have been utilized to achieve this goal in the visible spectrum [1]. circular split rings in the infrared [2] self-complementary rings [3] rectangular loops with diagonal microstrips [4], Different structures, V-shaped patches [5], inverted L-shaped resonators in diagonals [6] and circular patches along the diagonal [7]. A reflective anisotropic metasurface-based multifaceted broadband polarization rotator [8]. Multilayer structures, on the other hand, are typically incompatible with modern planar polarization control devices.

To create miniaturized polarization control devices with wide bandwidths and stable responses, it is necessary to develop artificial structures. One type of engineered electromagnetic structures that have been widely researched are metamaterials [9, 10]. These structures utilize periodic sub-wavelength patterning to achieve macroscopic responses that are not found in natural materials. Metasurfaces [11,12], which are two-dimensional analogs of metamaterials, have gained increased attention for their ability to Metasurfaces have gained significant attention in recent years as a means of controlling the polarization of electromagnetic waves. Anisotropic [13-16] and chiral metamaterials [17] have been extensively studied due to their unique electromagnetic properties, including bi-anisotropy, magneto-electric coupling, and elliptical or circular dichroism, in both linear [18, 19] and circular polarization [20, 21].

In this work a broadband polarization converter composed of a split ring resonator (SRR) with a circular split ring resonator (C- SRR) in the middle as a unit cell on the top surface of a metal-backed FR4 dielectric substrate is presented. The objective of this paper is to introduce an electrically thin metasurface that provides broadband polarization conversion for both normal and oblique incidences. The proposed design utilizes an anisotropic unit cell structure to achieve cross polarization along the u- and v-axes, and extends the operating bandwidth through three plasmonic resonances. The proposed metasurface has three distinctive characteristics: the substrate has a very small thickness, the unit cell structure is unique, and the unit cell size is sub-wavelength. These features enable the metasurface to have the same response for both x- and y- polarization and remain insensitive to incidence angles up to 60°.

2. DESIGN AND ANALYSIS

2.1 Unit Cell Configuration

The proposed 2-D cross polarization conversion metasurface's geometrical structure is given in Fig. 1(a).

The metasurface is composed of a two-dimensional periodic array of split ring resonators (SRRs) with a circular split ring resonator (C-SRR) in the middle, which is placed on top of the dielectric substrate. The structure is backed by a metallic plane. The unit cell of the proposed metasurface is displayed in Fig. 1(b). The unit cell consists of split ring resonator (SRR) with two split placed within the perpendicular sides, inside of which the splitted circular copper patches are printed over a copper-backed FR4 dielectric layer ($\epsilon_r = 4.4$ and $\tan \delta = 0.02$). Fig. 1(c) depicts the unit cell's schematic in three dimensions. This physical arrangement of the cell makes the metasurface very efficient for cross-polarization conversion of the incident wave. Cross-polarization conversion happens when an incoming electromagnetic wave with x-polarization gets transformed into a y-polarized wave (and vice versa) upon reflecting from the metasurface.

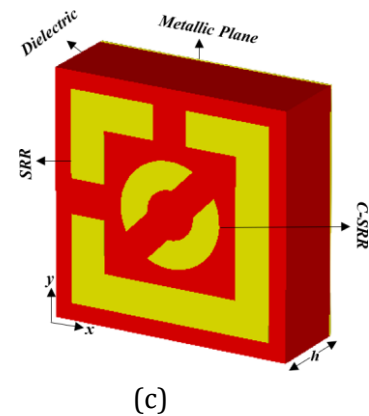
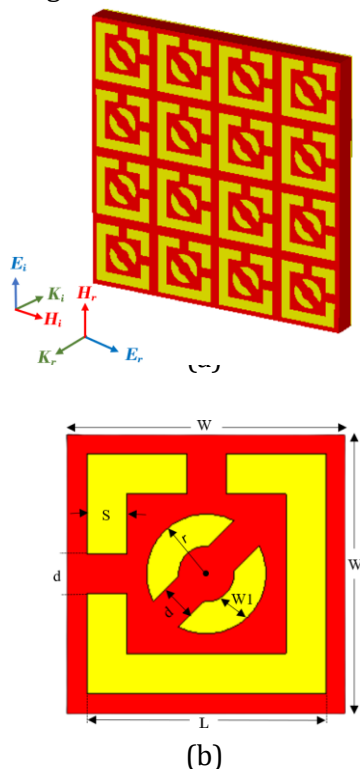


Fig. 1. (a) An overall diagram representing the proposed metasurface. (b) the unit cell from the top (c) A 3D representation of the unit cell.

In general, when an incident field has only one component, the reflected field usually contains both x and y components. The co-polarized reflection coefficients are determined by the magnitudes of the reflected electric field components parallel to the incident electric field $|R_{xx}| = |E_{rx}|/|E_{ix}|$ and $|R_{yy}| = |E_{ry}|/|E_{iy}|$. On the other hand, the cross-polarized reflection coefficients are determined by the magnitudes of the reflected electric field components perpendicular to the incident electric field $|R_{yx}| = |E_{ry}|/|E_{ix}|$ and $|R_{xy}| = |E_{rx}|/|E_{iy}|$, R_{yx} is the reflection coefficient when the incident field E_i is the x-polarized while the reflected field E_r is the y-polarized and R_{xy} The reflection coefficient occurs when the incident field is y-polarized, with the reflected field being x-polarized.

3. OPERATING PRINCIPLE

The metasurface is composed of a periodic arrangement of subwavelength unit cells that have the ability to be electrically or magnetically polarized. This allows the surface to be modeled as a collection of polarizable particles [22]. The electric and magnetic polarizabilities ($\alpha_{e,m}$) of each particle in the metasurface can be characterized. These polarizabilities are defined as the ratio of the electric dipole moment and magnetic dipole moment to the local average electric and magnetic fields, respectively. The average electric and magnetic fields can be related to the electric and magnetic dipole moments, through

$$\begin{bmatrix} \mathbf{P} \\ \mathbf{m} \end{bmatrix} = \begin{bmatrix} \alpha_{ee} & \alpha_{em} \\ \alpha_{me} & \alpha_{mm} \end{bmatrix} \begin{bmatrix} \mathbf{E} \\ \mathbf{H} \end{bmatrix} \quad (1)$$

where $\mathbf{p} = [p_x, p_y]^T$ is the electric dipole moment and $\mathbf{m} = [m_x, m_y]^T$ is the magnetic dipole moment, while the average tangential electric and magnetic fields at the metasurface are represented by $\mathbf{E} = [E_x, E_y]^T$ and $\mathbf{H} = [H_x, H_y]^T$. The time varying electric and magnetic polarization of the metasurface leads to the generation of electric and magnetic surface currents, which is given by

$$\begin{bmatrix} \mathbf{J} \\ \mathbf{M} \end{bmatrix} = i\omega \begin{bmatrix} \alpha_{ee} & \alpha_{em} \\ \alpha_{me} & \alpha_{mm} \end{bmatrix} \begin{bmatrix} \mathbf{E} \\ \mathbf{H} \end{bmatrix} \quad (2)$$

where $\mathbf{J} = [J_x, J_y]^T$ and $\mathbf{M} = [M_x, M_y]^T$ are The surface current densities for the electric and magnetic components are denoted by \mathbf{J} and \mathbf{M} , respectively, while ω represents the angular frequency of the incident electromagnetic wave Here, we are considering a time harmonic form of $e^{i\omega t}$. The relation between the surface current density \mathbf{J} and radiated far fields is given by [23]

$$\mathbf{E} = -i \frac{\omega \mu}{4\pi R} \int \mathbf{J}(x, y) \frac{e^{-ikR}}{R} dx dy \quad (3)$$

The integration is to be executed at the metasurface's surface. R is the separation between the observation point and the integration point. Eq. (3) shows that the direction of the radiated electric field and the surface current is the same. The generation of a y-polarized electric field requires the surface current to be in the y-direction. To achieve cross-polarization conversion, it is essential that the metasurface responds differently to incident electromagnetic waves that are polarized orthogonally to each other. Specifically, when an electric field with x-polarization is incident upon the metasurface, it should cause current flow in the y-direction, whereas when a y-polarized electric field is incident, current flow should occur in the x-direction.

The SRRs have been the subject of numerous studied in the literature. [24–26] It is shown [27,28] that a magnetic field passing through a sub-wavelength SRR loop can cause a magnetic as well as electric polarization. An important observation is that an electric field applied on the non-split side of the SRR

generates current only on that side. Conversely, if the field is applied along the split-bearing side, it can also create current on the perpendicular non split-bearing side of the SRR [27]. Usually, there is phase difference between the currents in the split and non-split-bearing sides. Consequently, at resonance, the net current flow in the direction perpendicular to the incident electric field is maximized, resulting in excellent cross-polarization.

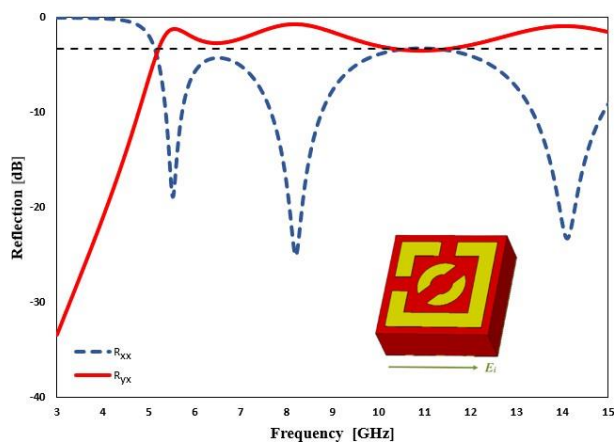
4. SIMULATED RESULTS AND PARAMETRIC ANALYSIS

In CST MICROWAVE STUDIO, the proposed structure is simulated using periodic boundary conditions. The optimized physical dimensions of the unit cell are given as follows in millimeters: $W = 7$, $L = 6$, $d = 1$, $S = 1$, $r = 1.5$, $W1 = 0.8$ and $h = 2.4$. The metasurface was design using copper for the SRRs and the ground plane with a conductivity of 5.8×10^7 S/m and a thickness of 0.035 mm. The utilized dielectric is FR4, which has a relative permittivity of 4.4 and a loss tangent of 0.02.

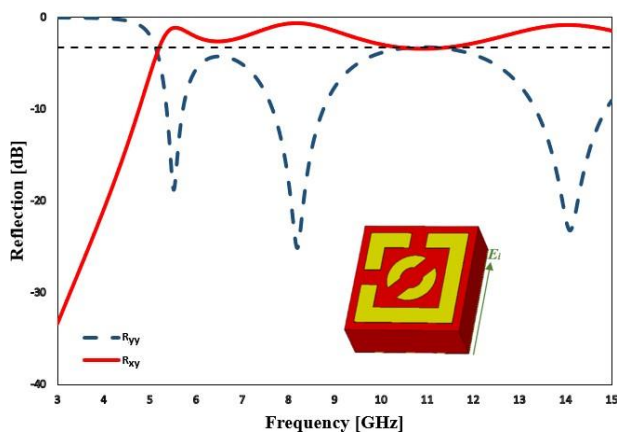
The co- and cross-polarized reflection coefficients are shown for normal incidence of an x-polarized incident field. in Fig. 2(a). It is clear from Fig. 2(a) The reflection coefficients for co-polarization were found to be lower than those for cross-polarization, with the cross-polarized reflection coefficient magnitude exceeding -3dB in two frequency bands 6-9.9 GHz and 11.7-15 GHz. The transmission coefficient of a metasurface backed by copper cladding is zero due to the perfect reflection of electromagnetic waves at the copper interface. As illustrated in Fig. 2(a), resonances take place at 5.5, 8.2, and 14.1 GHz. At these resonant frequencies, the co-polarized reflection coefficient drops to a very low value of -26dB, while the cross-polarized reflection coefficient approaches its maximum value of 0 dB. From the results, results, it can be inferred that an incoming wave polarized in the x-direction is entirely converted into a wave polarized in the y-direction after reflection from the metasurface.

Figure 2(b) displays the co-polarized and cross-polarized reflection coefficients for normal incidence of a y-polarized incident field on the metasurface at resonance frequencies. The co-polarized reflection coefficient exhibits a minimum value of -18.8 dB, -25 dB, and -23 dB at 5.5 GHz, 8.2 GHz, and 14.1 GHz, respectively, similar to the case of x-polarized waves.

Meanwhile, the cross-polarized reflection coefficient approaches 0 dB. The metasurface exhibits an identical response to both x and y-polarized waves, as demonstrated in Figures 2(a) and 2(b), wherein both polarizations are converted into their corresponding cross-polarized waves via the same way. Furthermore, for both TE and TM polarizations, the structure resonates at the same three distinct frequencies.



(a)



(b)

Fig. 2. The co-polarized and cross-polarized reflection coefficients' amplitudes can be calculated for an incident electromagnetic wave with (a) x-polarization and (b) y-polarization.

The polarization conversion ratio (PCR) can be defined as follows:

$$PCR = \frac{|R_{xy}|^2}{|R_{xy}|^2 + |R_{xx}|^2} \quad (4)$$

Fig.3 The suggested design demonstrates an almost perfect polarization conversion ratio of 100% at resonance frequencies of 5.5 GHz, 8.2 GHz, and 14.1 GHz. At these three resonant frequencies, the reflected wave with y-polarization is achieved by converting the incident wave with x-polarization entirely, and vice versa.

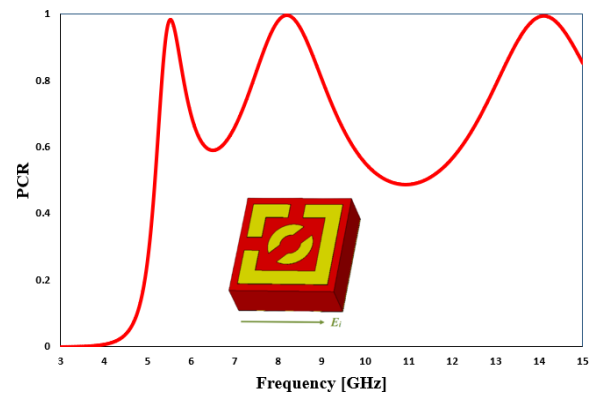
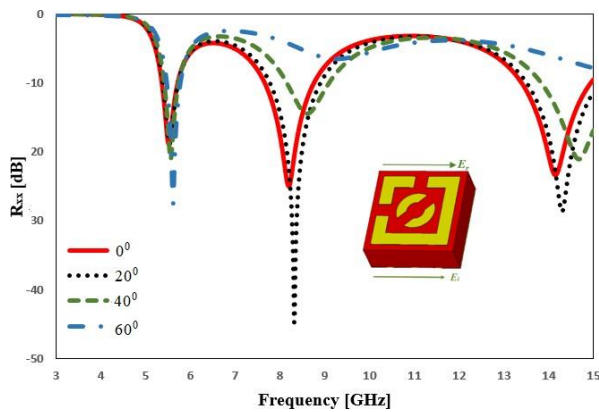


Fig. 3. Polarization conversion ratio (PCR).

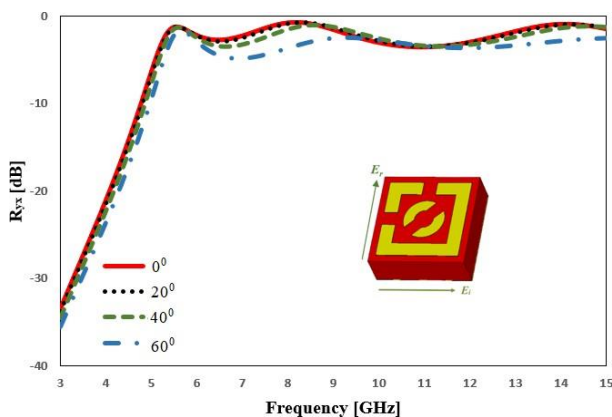
To ensure that a cross-polarization-conversion (CPC) metasurface can be useful across a range of applications, it is important that its response remains stable against different incidence angles. This means that the proposed structure needs to be able to achieve cross-polarization conversion and behave like a perfect magnetic conductor (PMC) for one component, while simultaneously acting like a perfect electric conductor (PEC) for the other. If the proposed metasurface is able to maintain a stable response for different incidence angles, then the resulting CPC will also be stable.

Typically, a high-impedance surface (HIS) with a thin dielectric substrate (h/λ smaller) has greater angular stability than one with a thicker substrate [28], [29]. While using a substrate with a high dielectric constant may also improve angular stability, this can result in a reduction in bandwidth [30].

To establish the stability of the suggested metasurface, Figure 4 exhibits the amplitudes of co-polarized and cross-polarized reflection coefficients at various incidence angles, given an x-polarized incident field (or TM polarization).



(a)

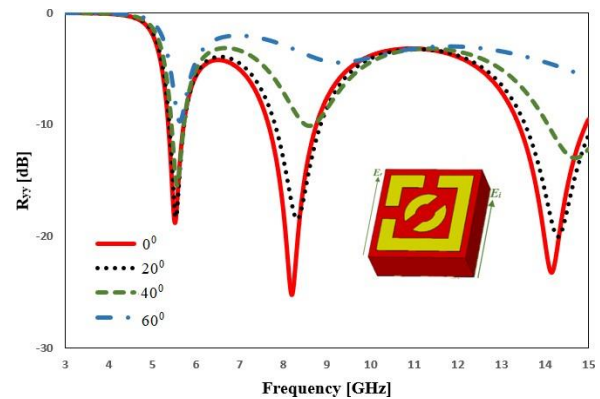


(b)

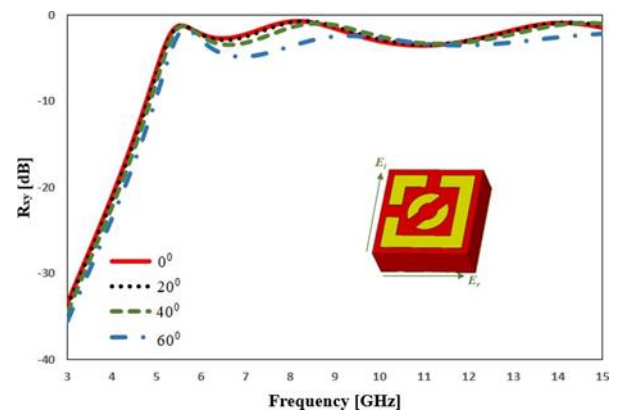
Fig. 4. (a) The reflection coefficient for co-polarization, and (b) the reflection coefficient for cross-polarization when the incident field is x-polarized.

The performance and bandwidth of cross-polarized reflection are stable against variations in incidence angle, as depicted in Fig. 4(b). The impact of incidence angle on the metasurface's functionality is minimal. At large incidence angles, the electric field passing through the SRR loop disturbs the surface current distribution on the metallic unit cell, which leads to minor variations in the cross-polarized reflection, considering the incident polarization as transverse magnetic (TM). Figures display the co-polarized and cross-polarized reflection coefficients for various incidence angles in Figs. 5(a) and 5(b), respectively, when the incident wave is polarized in the y-direction (TE polarization). For TE-polarized incident waves, the magnetic field passing through the SRR loop at large incidence angles disturbs the current flow, resulting in minor variations in the cross-polarized reflection. Nevertheless, these effects are counteracted by the currents on the SRR and the cross-element,

stabilizing the response and keeping the variations within acceptable limits.



(a)



(b)

Fig. 5. (a) The reflection coefficient for co-polarization, and (b) the reflection coefficient for cross-polarization when the incident field is y-polarized.

To understand the physical mechanism behind cross-polarization conversion, the proposed design is simulated under u- and v-polarizations to examine its reflection coefficient (magnitude) and surface current distribution. Fig. 6 displays the reflection coefficient magnitude for u and v-polarized waves. The co-polarized reflection coefficient's magnitude is nearly 0 dB for both u- and v-polarized waves across the desired frequency bands. While the magnitude of the co-polarized reflection coefficient reaches 2.6 dB at 5.5 GHz for u-polarization, it is still considered within an acceptable range.

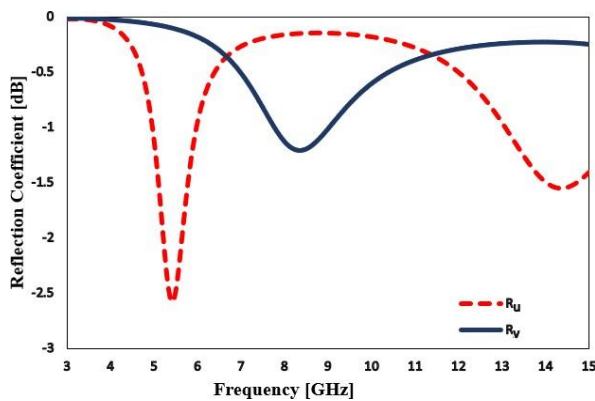
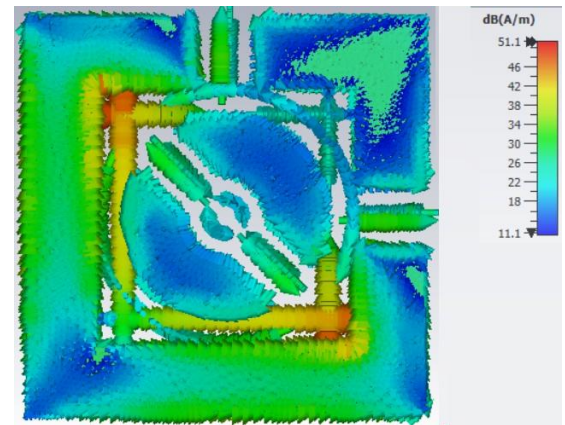
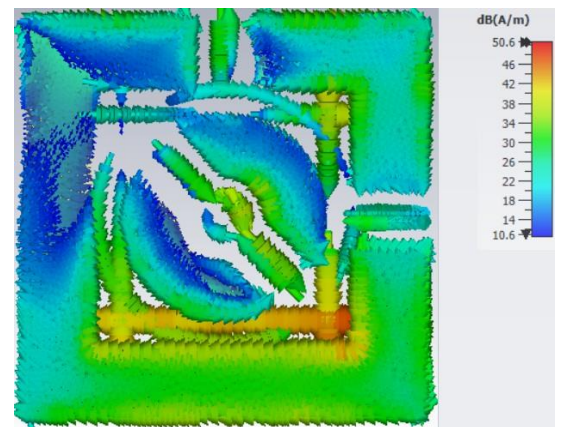


Fig. 6. Co-polarized reflection coefficient (a) magnitude.

Figure 6's plot of the magnitude of the reflection coefficient exposes that the two resonances (manifested as dips in the reflection coefficient's magnitude) occurring at 5.5 GHz and 14.1 GHz are a consequence of the u-polarized wave. Meanwhile, the third resonance at 8.2 GHz is due to the v-polarized incident electric field. In addition, the suggested design shows no cross-polarization conversion for u- and v-polarized waves since the co-polarized reflection is substantial in the case. Interestingly, the structure's anisotropy leads to polarization-selective cross-polarization conversion, enabling only x- and y-polarized waves to convert into their corresponding orthogonal polarizations. Fig. 7 provides additional physical insights into the electromagnetic behavior of the proposed metasurface unit cell through surface current distribution analysis. The figure displays the surface current density in vector form at three plasmon resonances (5.5, 8.2, and 14.1 GHz) for a y-polarized incident wave.



(b)

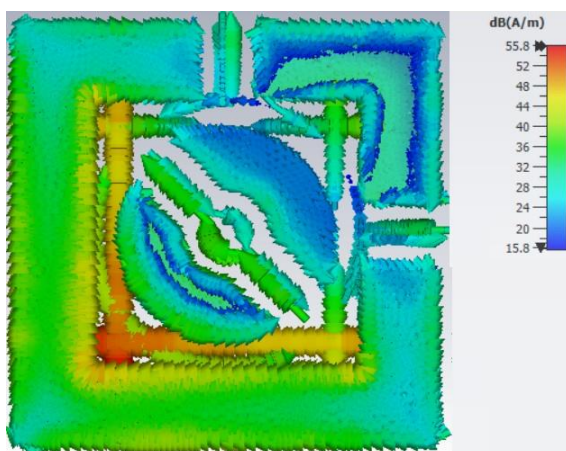


(c)

Fig. 7. Surface current distribution (a) 5.5 GHz (b) 8.2 GHz (c) 14.1 GHz

5. CONCLUSIONS

This paper introduces a thin dual broadband cross-polarization conversion metasurface operating in the microwave frequency range. The proposed metasurface successfully converts x-polarized waves into y-polarized waves and vice versa over two frequency bands, namely 6–9.9 GHz and 11.7–15 GHz, with a polarization conversion efficiency of 73% at three plasmonic resonances (5.5 GHz, 8.2 GHz, 14.1 GHz). The cross-polarization conversion efficiency of metasurface remains consistent for both types of polarization and is insensitive to the incidence angle up to 60 degrees. This is due to the subwavelength unit cell size of 0.1λ at 5 GHz, making it independent of the angle of incidence and polarization of the incoming wave. The proposed metasurface can find applications in polarization control devices and other areas requiring cross-polarization conversion.



(a)

REFERENCES

- [1] Y. Zhao, A. Alu, Nano Letters **13**(3), 1086 (2013).
- [2] P. E. Sieber, D. H. Werner Werner, Opt. Express **21**(1), 1087 (2013).
- [3] L. Wu, M. Zhang, B. Zhu, J. Zhao, T. Jiang, Y. Feng, Appl. Phys. B **117**(2), 527 (2014).
- [4] H. L. Zhu, W. Cheung, X. H. Liu, T. I. Yuk, IEEE Trans. Antennas Propag. **62**, 2891 (2014)
- [5] uozhi Zhao, Shihua Bi, Yancheng Cui, AIP Advances **9**, 075016 (2019).
- [6]] Y. Jia, Y. Liu, W. Zhang, S. Gong, Applied Physics Letters **109**(5), 051901 (2016).
- [7] K. Srivastava, B. Mishra, R. Singh, International Journal of Microwave and wireless technologies, **14**(4), 502 (2022).
- [8] A. Ahmed, Q. Cao, M. I. Khan, F. Ahmed, F. A. Tahir, Physics Letters A **470**, 128785 (2023).
- [9] V. G. Veselago, Soviet Phys. Uspekhi **10** (4), 509 (1968).
- [10] J. B. Pendry, Phys. Rev. Lett. **85**, 3966 (2000).
- [11] M. Y. Shalaginov, S. D. Campbell, S. An, Y. Zhang, C. Ríos, E. B. Whiting, Y. Wu, L. Kang, B. Zheng, C. Fowler, H. Zhang, D. H. Werner, J. Hu, T. Gu, Nanophotonics **9** (11), 3505 (2020).
- [12] S. Sun, Q. He, J. Hao, S. Xiao, L. Zhou, Advances in optics and Photonics **11** (2), 380 (2019).
- [13] C. Pfeiffer, A. Grbic, Phys. Rev. Appl. **2** 044011 (2014).
- [14] R. Xia, X. Jing, X. Gui, Y. Tian, Z. Hong, Opt. Mater. Express **7** (3) 977 (2017).
- [15] R. Li, Z. Guo, W. Wang, J. Zhang, A. Zhang, J. Liu, S. Qu, J. Gao, Opt Express **22**(23), 27968 (2014).
- [16] Y. Zhao, X. Cao, J. Gao, X. Liu, S. Li, Opt. Express **24** 11208 (2016).
- [17] Y. Wang, Rongcao, Y. Zhao, J. Tian, Optics Communication **530**, 129196 (2023).
- [18] Muhammad Ismail Khan, Qaisar Farz, Farooq A. Tahir, Journal of Applied Physics **121**, 045103 (2017).
- [19] J. H. Shi, H. F. Ma, C. Y. Guan, Z. P. Wang, T. J. Cui, Phys. Rev. B **89**, 165128 (2014).
- [20] X. Gao, X.- Y. Yu, W.- P. Cao, Yan-Nan Jiang, Xin-Hua Yu, Chin. Phys. B **25**, 128102 (2016).
- [21] Shah, S.M.Q.A., Shoaib, N., Ahmed, F. et. al., Sci Rep **11**, 1774 (2021).
- [22] H. L. Zhu, S. W. Cheung, K. L. Chung, T. I. Yuk, IEEE Trans Antennas Propag. **61**, 4615 (2013).
- [23] E. F. Kuester, M. A. Mohamed, M. Piket-May, C. L. Holloway, IEEE Trans. Antennas Propag. **51**(10), 2641 (2003).
- [24] C. A. Balanis, Antenna Theory: Analysis and Design), 142 (John Wiley & Sons), (2016).
- [25] N. Katsarakis, T. Koschny, M. Kafesaki, E. N. Economou, C. M. Soukoulis, Appl. Phys. Lett. **84**(15), 2943 (2004).
- [26] J. Y. Yin, X. Wan, Q. Zhang, T. J. Cui, Sci. Rep. **5**, 12476 (2015).
- [27] S. Zahertar, A. D. Yalcinkaya, H. Torun, AIP Adv. **5**, 117220 (2015).
- [28] Peter De Maagt, Constantin R. Simovski and I.V.Melchakova, IEEE Trans. Antennas Propag., **53**(3), 908 (2005).
- [29] Edward F. Kuester, IEEE transactions on Antenna and Propagation (2019).
- [30] O. Luukkonen, F.Costa, C. R. Simovski, A. Monorchio, S. A. Tretyalov, IEEE Transactions on Antennas Propagation, **57**(10), 3119 (2009).